Activated Carbon Fibre Monoliths for Hydrogen Storage

Mirko Kunowsky[1,a], Juan Pablo Marco-Lozar[1,2,b] and Ángel Linares-Solano[1,c*]

[1]Grupo de Materiales Carbonosos y Medio Ambiente, Departamento de Química Inorgánica, Universidad de Alicante, Ap. 99, 03080 Alicante, Spain

[2]Gas to Materials Technologies S.L., 03001 Alicante, Spain

[a]kunowsky@ua.es, [b]juanp.marco@ua.es, [c]linares@ua.es

* corresponding author

Keywords: Hydrogen storage, porous adsorbents, activated carbon, density, adsorption

Abstract. Porous adsorbents are currently investigated for hydrogen storage application. From a practical point of view, in addition to high porosity developments, high material densities are required, in order to confine as much material as possible in a tank device. In this study, we use different measured sample densities (tap, packing, compacted and monolith) for analyzing the hydrogen adsorption behavior of activated carbon fibres (ACFs) and activated carbon nanofibres (ACNFs) which were prepared by KOH and CO_2 activations, respectively. Hydrogen adsorption isotherms are measured for all of the adsorbents at room temperature and under high pressures (up to 20 MPa). The obtained results confirm that (i) gravimetric H_2 adsorption is directly related to the porosity of the adsorbent, (ii) volumetric H_2 adsorption depends on the adsorbent porosity and importantly also on the material density, (iii) the density of the adsorbent can be improved by packing the original adsorbents under mechanical pressure or synthesizing monoliths from them, (iv) both ways (packing under pressure or preparing monoliths) considerably improve the storage capacity of the starting adsorbents, and (v) the preparation of monoliths, in addition to avoid engineering constrains of packing under mechanical pressure, has the advantage of providing high mechanical resistance and easy handling of the adsorbent.

Introduction

The storage of hydrogen and methane (natural gas) has received great attention, since many years ago, because both gases are efficient clean fuels with no carbon emission (hydrogen) and acceptable low carbon emissions (methane). More recently, the storage interest has also reached carbon dioxide in relation to environmental applications (capture and transportation) [1-6]. Among these three gases, the storage of hydrogen is the most difficult task, due to its special physical and chemical characteristics [7,8]. Four methods are available to store hydrogen: compressed gas, liquid hydrogen, metal hydrides, and high pressure adsorption on highly porous adsorbents (several MPa to 70 MPa, at ambient temperature or at cryogenic ones) [9-14]. Among them, the high pressure adsorption process is a promising alternative, presenting advantages such as: short refueling times, fast kinetic of storage and release (reversibility), low heat evolution, and efficient cyclability. Additionally, high pressure adsorption is very much depending on the surface area, porosity and pore size of the adsorbent and there is a large variety of porous solids (*e.g.*, zeolites, highly activated carbons, activated carbon nanotubes, zeolite template carbons, carbide-derived carbons, metal organic frameworks (MOFs) and covalent organic frameworks (COFs)). In all of them, their porosity, surface area, morphology, size and shape are tunable and, hence, able for further improvements.

Since many years ago our research group has been developing highly microporous activated carbons for high pressure adsorption (supercritical gas adsorption for H_2 and CH_4 and subcritical gas adsorption for CO_2, see for example the chapters in [15-23] and the references therein). In these

works, as well as in most published ones, gas storage (expressed per unit of weight of the material; *i.e.*, on gravimetric basis) correlates well with the adsorbent porosity, although the nature of the gas, the temperature, and the pressure used influence the resulting correlations. Considering that the adsorbent has to be confined in a vehicle tank with limited volume and that the density of the adsorbent depends very much on its porosity, the storage capacity of a given adsorbent should also be reported per unit of volume of adsorbent (*i.e.*, on volumetric basis), as it was pointed out a long time ago (1994) by Chahine et al. [24].

In our previous works, it was demonstrated that the density of the adsorbent is a critical parameter for hydrogen storage application by physisorption [4-6,15,17,22,23,25]. Thus, the packing density of the adsorbent affects directly the excess adsorption on a volumetric basis. Furthermore, and even more important from an application point of view, the adsorbent density is a key factor which controls the total quantity of hydrogen that can be stored in a given volume [4,15,20,25]. This is especially important for hydrogen storage at room temperature, where the contribution of the compressed hydrogen in the void space is considerable and has to be taken into account [4,25].

In the present work, the influence of the adsorbent density is further studied and optimized for hydrogen adsorption at room temperature. As adsorbents, different activated carbon fibres (ACFs), activated carbon nanofibers (ACNFs), and monoliths produced from them are investigated. In the cases of the ACFs and ACNFs different models are considered for filling them in the tank: (i) at atmospheric pressure (tap density), (ii) by packing under mechanical pressure (packing density), and (iii) packing under pressure and releasing it (compacted density). In the case of the monoliths, their densities are obtained from their dimensions, without using any compression. The ACF and ACNF precursors and the monoliths are compared with each other regarding their densities, their porosities, and their hydrogen adsorption isotherms.

Materials and experimental methods

Activated carbon fibres (ACF). Three ACFs, kindly provided by Nippon Kynol Inc., (Gun-Ei Chemical Industry Co., Ltd., Japan), were used: Kynol ACF-1603-15, Kynol ACF-1603-20, and Kynol ACF-1603-25. These ACFs (identified as ACF15, ACF20, and ACF25) were produced from a phenolic resin (novoloid). Additionally, two commercial carbon fibres, provided by Donacarbo at two different carbonization temperatures (1000ºC and 700ºC), were activated with different KOH-ratios at 1023 K in a chamber furnace, as described elsewhere [26] (samples D10 and D7).

Activated carbon nanofibres (ACNF). An amorphous carbon nanofibre which was prepared by Prof. A. Oya by using his polymer blend technique and spinning [27,28], was activated with 100 ml min^{-1} of CO_2 at 1073 K during 24 h (sample ACNF) [29].

ACF and ACNF monolith preparation. The monoliths investigated in this study were produced by mixing the carbon fibres or the carbon nanofibres with water and a polymeric binder [29,30]. The binder was available as a 55 % aqueous solution of polyvinylidene chloride (PVDC) (Waterlink Sutcliffe Carbons, UK). Different binder/carbon material ratios (on a weight basis) were used, but, for space limitation, we are going to analyze only the 1/1 ratio. The binder/carbon mixture was heated at around 363 K for 24 h, and afterwards the dry mixture was ground and introduced into a cylindrical piston mold. The mold was installed in a mechanical press. Here, the mixture was compressed progressively, until reaching an equivalent pressure, corresponding to 3.5 tonne. The mold was then heated up to 413 K and, upon reaching this temperature, the heating device was turned off, and the mold was cooled down by convection before removing it from the press. Finally, the obtained monoliths were carbonized under a N_2 flow of 100 ml min^{-1} in a horizontal tube furnace. The furnace was heated stepwise and with low heating rates of 2 K min^{-1}, in order to ensure the removal of any gaseous reaction products and to prevent the disruption of the monolith. At

448 K and at 723 K the temperatures were maintained constant for 1 h, and at the maximum temperature of 1023 K for 2 h. Subsequently, the furnace was cooled down by convection.

Porosity characterization. Sub-atmospheric gas adsorption measurements (of N_2 at 77 K and of CO_2 at 273 K) were carried out in a Quantachrome Autosorb 6. Previously, the samples were degassed at 523 K for 4 h under vacuum. The apparent BET surface areas (S_{BET}) were calculated, and the total micropore volumes ($V_{DR}(N_2)$) and narrow micropore volumes ($V_{DR}(CO_2)$) were obtained from Dubinin-Radushkevich (DR) equation. In order to get representative samples, the monoliths were crashed, grounded, and mixed previous to their porosity characterization.

Density characterization. The densities of the monoliths (ρ_{mono}) were obtained from their weight and from their volume, using a caliper rule to measure their diameters and heights. Different densities of the ACF and ACNF samples (ρ) were measured under different conditions in a mechanical press. Thus, a mass of typically 0.5 g of sample was introduced into a cylindrical steel mould with a diameter of 13 mm. A tightly fitting steel piston was introduced into the mould, and the assembly was installed into the press. The tap density (ρ_{tap}) was measured without applying compacting pressure; thus, it corresponds to the volume which is occupied by the loose sample. The packing density (ρ_{pack}) was measured while a force, equivalent to the mass of 1 tonne, was applied on the samples via the piston. For a piston diameter of 13 mm, this results in a pressure of 73.9 N mm^2. The compressed density (ρ_{comp}) was obtained after removing the applied force. The piston heights were measured with a caliper rule. In order to measure the reference height, a blank measurement without sample was performed. The volume occupied by the sample was calculated by Eq. 1, taking into account the difference of the heights from experiment and reference (Δh), the sample mass (m), as well as the piston diameter ($\emptyset$).

$$\rho = 4 \bullet m / (\emptyset^2 \bullet \pi \bullet \Delta h) \quad (1)$$

High pressure hydrogen adsorption. Hydrogen adsorption isotherms at 298 K and up to 20 MPa were measured in a fully automated volumetric device which was designed and built at University of Alicante (described in more detail in [26]) and which is now commercialized by Quantachrome (iSorbHP1). For the measurements, around 0.5 g of sample were used which were degassed beforehand at a temperature of 423 K for 4 h under vacuum. Hydrogen adsorption amounts on both, gravimetric and volumetric terms, as well as the total H_2 storage amounts were calculated due to the formulas explained in a previous work [25].

Scanning electron microscopy. For scanning electron microscopy (SEM) a Hitachi S-3000N was used, with an electron acceleration voltage of 20 kV. Secondary electrons were detected by a scintillator-photomultiplier (Everhart-Thornley detector) which has a resolution of 3.5 nm.

Results and discussion

SEM images of ACFs and ACNFs. The morphology and sizes of the three types of activated fibrous carbons used can be seen in Fig. 1 that presents the SEM images of one sample of each type: ACF15, D10 and ACNF. The morphology and sizes of sample ACF15 are very similar to the ones of ACF20 and ACF25 (SEM images not shown). Their diameters range from approximately 5 to 20 µm, typically having a value around 10 µm. The same occurs, comparing SEM images of D10 and D7 (SEM images not shown) which both reveal diameters between 10 and 30 µm and uniform lengths of 100 to 300 µm. The ACNFs present a homogeneous surface and have nanometric diameters between 100 and 200 nm. Interestingly, in the case of all investigated samples, neither CO_2 nor KOH-activation destroys the fibrous structures of the original fibers and does not change their dimensions, indicating that activations took place uniformly within the bulk of the fibers.

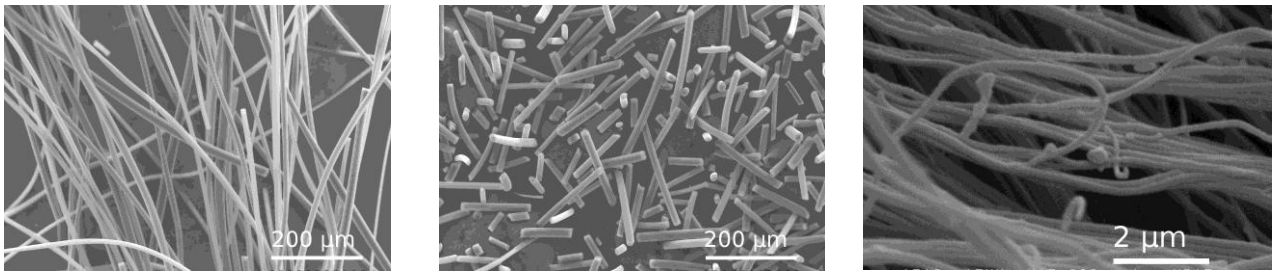

(a) (b) (c)

Fig. 1: SEM images of the activated carbon fibre and nanofibre precursors: (a) ACF15, (b) D10, and (c) ACNF.

Table 1: Porous texture and density results of the ACFs and ACNFs precursors.

Sample	S_{BET} [m^2g^{-1}]	$V_{DR}(N_2)$ [cm^3g^{-1}]	$V_{DR}(CO_2)$ [cm^3g^{-1}]	ρ_{tap} [g cm^{-3}]	ρ_{pack} [g cm^{-3}]	ρ_{comp} [g cm^{-3}]
ACF15	1193	0.56	0.52	0.24	0.94	0.64
ACF20	1674	0.75	0.43	0.20	0.73	0.43
ACF25	1989	0.87	0.62	0.17	0.76	0.44
D10	2259	0.97	0.71	0.36	0.62	0.43
D7	2364	1.02	0.79	0.34	0.63	0.44
ACNF	1910	0.87	0.59	0.13	0.49	0.21

The porosity values (S_{BET}, $V_{DR}(N_2)$, and $V_{DR}(CO_2)$), as well as the densities of the ACFs and ACNFs used are given in Table 1. For the ACF15, ACF20, and ACF25 fibres it can be observed that the BET surface areas and total micropore volumes increase accordingly to their nomenclature (ACF15 < ACF20 < ACF25). Thereby, the S_{BET} values are 1200 m^2g^{-1}, 1700 m^2g^{-1} and close to 2000 m^2g^{-1}, and the $V_{DR}(N_2)$ values increase from 0.56 cm^3g^{-1} to 0.87 cm^3g^{-1}. The analysis of the narrow microporosity (assessed form CO_2 adsorption) reveals important differences depending on the sample. As it is expected, the tap and packing densities decrease with the grade of activation. Thus, the tap densities decrease in the order ACF15 > ACF20 > ACF25, from a maximum value of 0.24 g cm^{-3} down to 0.17 g cm^{-3}. The packing density follows the same trend, with a maximum value of 0.94 g cm^{-3} for the ACF15 fibre, and a minimum value of 0.76 g cm^{-3} for the ACF25 fibre. In general, the Donacarbo fibres have a more developed porosity than the ACNF and Kynol fibres. Thus, D10 and D7 reach BET surface areas of 2260 and 2360 m^2g^{-1}, respectively, and total micropore volumes around 1 cm^3g^{-1}. The ACNF sample also reveals an interesting porosity which is

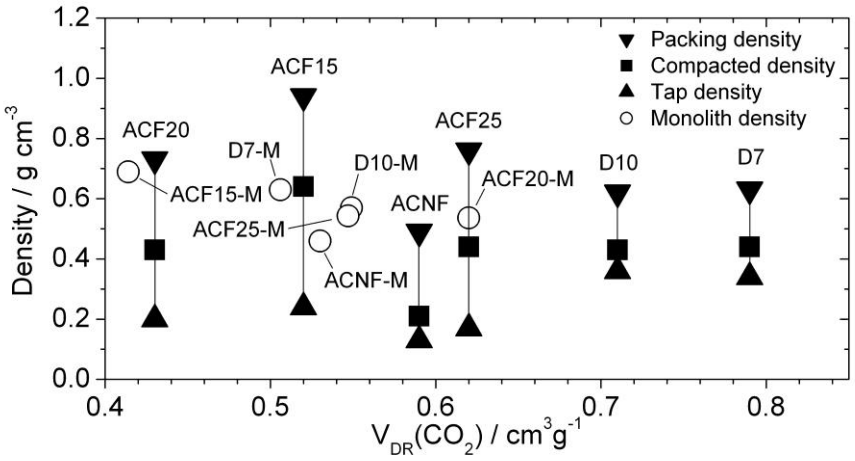

Fig. 2: Material densities of ACFs, ACNFs and of their corresponding monoliths, plotted over the volume of narrow micropores < 0.7 nm, $V_{DR}(CO_2)$.

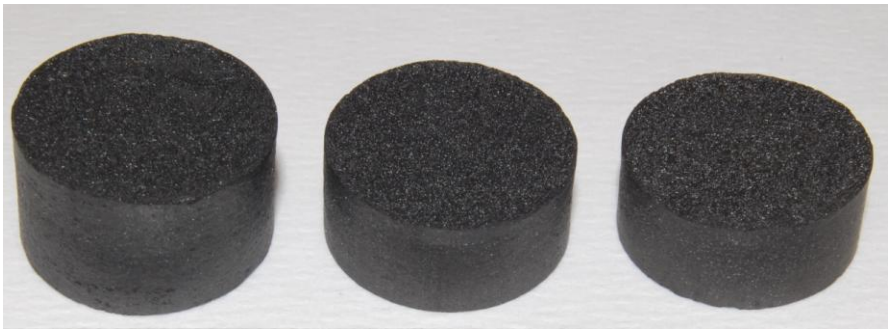

(a)

(b)

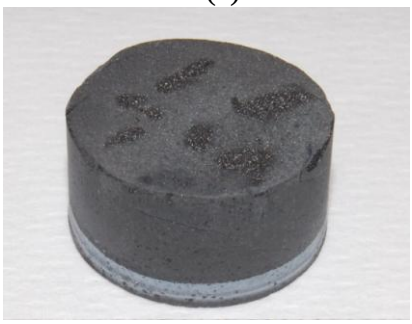

(c)

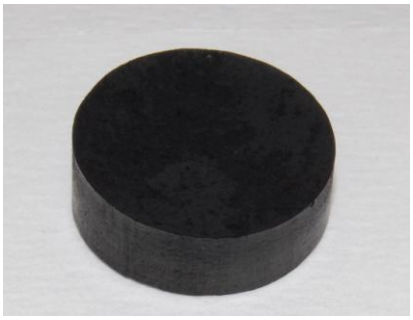

(d)

Fig. 3: Photographs of the synthesized monoliths with diameters of 13 mm each: (a) ACF25-M, ACF20-M, and ACF15-M; (b) D10-M; (c) D7-M; (d) ACNF-M.

similar to the ACF25 (*i.e.*, BET surface area close to 2000 m^2g^{-1} and a narrow micropore volume of 0.6 cm^3g^{-1}). Table 1 also shows that most of the samples have reasonable high volumes of narrow micropores which are the most suitable for hydrogen adsorption at room temperature [15,26], especially the Donacarbo ACFs which reach the highest values (0.7 and 0.8 cm^3g^{-1}).

In Fig. 2, the three different density values (packing, compacted and tap density) of each ACF and ACNF are plotted over the narrow micropore volume, $V_{DR}(CO_2)$. It can be observed that for each fibre material, the densities follow the order $\rho_{tap} < \rho_{comp} < \rho_{pack}$. The densities of the Kynol ACFs cover a larger range than the ACNF and the Donacarbo-based samples. Thus, they have lower tap densities than the latter, but, upon compacting, they reach similar or superior values, meaning that the Kynol fibres can be better optimized by mechanical pressure. In the case of the ACNF and the Donacarbo-based samples it can be observed that their compressed densities are very close to their tap densities. This reveals that these materials have a strong resiliency behavior [29].

ACF and ACNF monoliths. In Fig. 3, photographs of the synthesized monoliths are shown. All of them have mechanical stability and can be well managed. Fig. 3(a), from left to right, shows the monoliths ACF25-M, ACF20-M and ACF15-M which were synthesized from Kynol ACFs. Although all three monoliths were prepared similarly, with a 1/1 PVDC/fibre ratio, some differences can be observed. Thus, more compact and stable monoliths with fewer fissures on their surface can be produced from the less porous activated carbon fibres (*i.e.*, ACF15 and ACF20). The monoliths which were produced from the Donacarbo fibres D10 and D7 are shown in Fig. 3(b) and Fig. 3(c), respectively, and the monolith produced from the ACNF is shown in Fig. 3(d). All the prepared monoliths are very stable and have smooth surfaces without flaws or fissures; bright areas which can be observed on the external parts (especially on D7-M) are only superficial and originate from polymer seals used in the mechanical press.

The densities and porosity values for all of the synthesized ACF monoliths are compiled in Table 2 and also in Fig. 2 for comparison purpose. Interestingly, the monoliths reach remarkable density (ρ_{mono}) values. They are lower than the packing densities of the fibrous materials but, in

Table 2: Porous texture and density results of the ACFs and ACNFs monoliths.

Sample	S_{BET} [m^2g^{-1}]	$V_{DR}(N_2)$ [cm^3g^{-1}]	$V_{DR}(CO_2)$ [cm^3g^{-1}]	ρ_{mono} [$g\ cm^{-3}$]
ACF25-M	1838	0.78	0.55	0.54
ACF20-M	2068	0.89	0.62	0.54
ACF15-M	1127	0.52	0.41	0.69
D10-M	1855	0.78	0.55	0.57
D7-M	1532	0.69	0.51	0.63
ACNF-M	1450	0.65	0.53	0.46

general terms, they are higher than the tap and compressed densities of the original ACFs and ACNFs. Such unfavourable, lower density of the monoliths, in comparison with the packing densities, has its compensation: the advantage of being a more realistic value that could easily be achieved under practical conditions in a storage device. The porosity of the monoliths decreases when compared with the values reached by the pristine fibrous materials as it can be seen in Table 2. A special case is the ACF20-M monolith that gains porosity in relation to its ACF20 precursor. Regarding the narrow microporosity values, the differences between the monoliths are very small. In comparison with the Kynol-based monoliths, the drop of porosity is much more pronounced for the Donacarbo ACFs.

H_2 adsorption at 298 K. Fig. 4 presents, for a selection of samples (7 samples among the 12 studied), the excess hydrogen adsorption isotherms, expressed on a gravimetric basis. The isotherms of the 12 samples have been obtained at room temperature and up to pressures of 20 MPa. From them, the results of Table 3 have been calculated on gravimetric and on volumetric basis, and as the total H_2 storage capacities (THS). Fig. 4 and Table 3 show that the samples have different hydrogen adsorption capacities, depending on their different porosities. It has been well proved [15,26] that, depending on the adsorption temperature and on the pressure used, the hydrogen uptake depends on the sample properties (*i.e.*, the micropore volume (also the apparent BET surface area) or the narrow-micropore volume). At room temperature and pressures below 20 MPa the gravimetric H_2 excess adsorption is well related to the narrow micropore volume, giving a better relation the lower the pressure is. Fig. 5 plots the hydrogen uptake of the samples of Fig. 4 as a function of their narrow-micropore volumes at three pressures: 4 MPa, 10 MPa, and 20 MPa. We can observe that

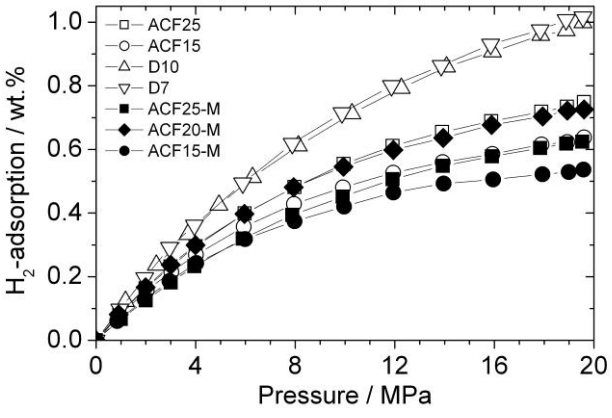

Fig. 4: H_2 excess adsorption isotherms on a gravimetric basis obtained at room temperature for a selection of ACFs and ACF monoliths.

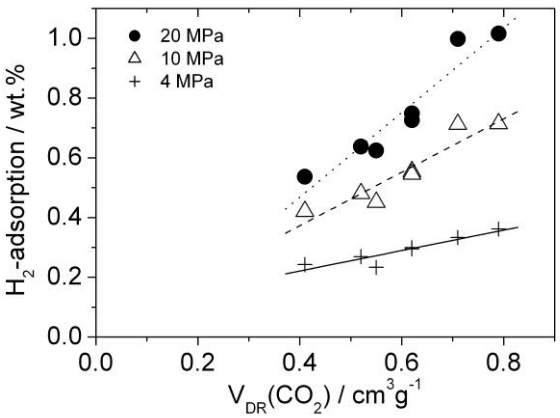

Fig. 5: Representation of the gravimetric H_2 excess adsorption amounts, obtained at room temperature and different pressures (4 MPa, 10 MPa, and 20 MPa), over the narrow micropore volumes for a selection of samples.

Table 3: Maximum H_2 adsorption and storage results obtained at 298 K and 20 MPa of ACFs, ACNFs and their monoliths.

Sample	H_2 adsorption		Total H_2 storage
	[wt.%]	[g l^{-1}]	[g l^{-1}]
ACF15	0.64	6.1	14.2
ACF20	0.75	5.6	15.1
ACF25	0.75	5.7	15.1
D10	1.00	6.3	16.5
D7	1.02	6.4	16.6
ACNF	1.26	6.3	17.4
ACF15-M	0.54	3.7	13.5
ACF20-M	0.73	3.9	14.4
ACF25-M	0.62	3.4	14.1
D10-M	0.95	5.5	16.1
D7-M	0.76	4.9	15.0
ACNF-M	1.02	4.2	15.8

the relationships are better for lower pressure. Anyway, these reasonable good relationships confirm that, at room temperature and < 20 MPa, the narrow-micropore volume of the adsorbent controls the hydrogen uptake, as it has been pointed out in previous works [4,6,15,26].

Fig. 6 presents, for the same set of samples of Fig. 4, their volumetric hydrogen uptakes (Fig. 6a) and their total H_2 storage (Fig. 6b), selecting in both cases the packing density or monolith density of the samples. It has to be pointed out that the hydrogen uptake order of Fig. 6 differs considerably of that of Fig. 4 which reveals the importance of the sample density used to assess the samples volumetric and THS uptakes. Furthermore, if the density of the sample used is different from the packing density or the monolith density, the results will be affected.

Thus, in order to further analyze the influence of the density used to calculate the hydrogen uptake, Fig. 7 presents the different volumetric hydrogen uptakes of a given sample (ACNF), using the three densities studied (tap, packing and compressed) and of its corresponding monolith, using its density (ρ_{mono}). In general, the hydrogen uptakes of the nanofibre-based samples (ACNF and ACNF-M) reach higher gravimetric adsorption amounts than the investigated ACFs of comparable porosities (see Tables 1, 2 and 3). Thus, ACNF reaches the highest gravimetric value (over 1.2 wt.%), even though it does not have the highest apparent BET surface area. The prepared monolith from the ACNFs (ACNF-M) presents the maximum value among the studied monoliths.

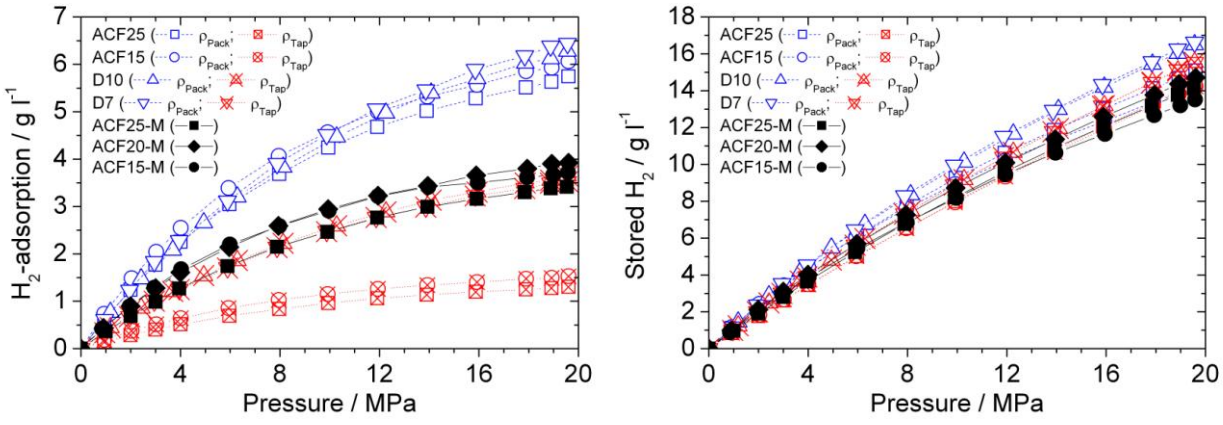

(a) (b)

Fig. 6: (a) H_2 excess adsorption isotherms and (b) total H_2 storage isotherms on a volumetric basis obtained at room temperature for a selection of ACFs and ACF monoliths. The results of the ACFs were obtained, taking into account both, packing and tap densities.

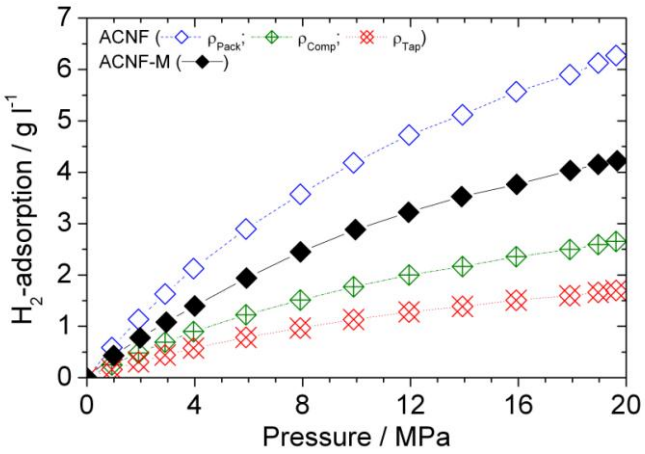

Fig. 7: H_2 excess adsorption isotherms on a volumetric basis obtained at room temperature for sample ACNF, taking into account its packing, compressed, and tap densities, as well as its monolith (ACNF-M), taking into account its monolith density.

Fig. 7 clearly shows that the volumetric hydrogen uptake (which is more important than the gravimetric for storage applications) increases, depending on the density used ($\rho_{tap} < \rho_{comp} < \rho_{mono} < \rho_{pack}$). Despite its exceptionally high gravimetric value, the ACNF sample reaches the lowest volumetric adsorption amount when ρ_{tap} is used, due to the low value of the latter. However, due to the high density increment of this material under mechanical pressure, a high value is reached if ρ_{pack} is taken into account. The monolith ACNF-M reaches a value which is higher than those of its precursor (ACNF) if ρ_{tap} or ρ_{comp} are used as adsorbent density, but lower if ρ_{pack} is taken into account. Therefore, Fig. 7 clearly points out the importance to well assessing the density of the sample [4] and of describing the experimental conditions used to measure it.

In Table 3, where the maximum H_2 adsorption amounts, obtained at 298 K and 20 MPa, of the investigated samples are resumed, and, in addition, also the total H_2 storage amounts are presented (calculated with the equations given in [25]), the monolith D10-M reaches the highest total storage capacity (16.1 g l^{-1}) among the studied ACF monoliths. This is achieved by a combination of high gravimetric adsorption amount and density. These findings corroborate the usefulness of monolith synthesis. Thus, it is demonstrated that, instead of using activated carbon fibres as they are, synthesizing monoliths from them can be advantageous for hydrogen storage application.

Conclusions

From the analysis of the hydrogen adsorption results obtained at room temperature up to 20 MPa as function of adsorbate density model used for filling the tank with the adsorbent (tap density, packing density, compacted density and monoliths preparation from different ACFs and ACNFs sorbents), the following conclusions can be reached: (i) The density can be significantly improved by a factor of 4 due to packing of the ACFs under mechanical pressure. However, under practical conditions, packing of the adsorbent may not be feasible, due to engineering constrains. Here, the synthesis of ACF monoliths or ACNF monoliths is beneficial. Furthermore, monoliths provide the additional advantages of high mechanical resistance and easy handling. (ii) Gravimetric H_2 adsorption is directly related to the porosity of the adsorbent, and maximum values over 1.2 wt.% are reached. (iii) Gravimetric H_2 adsorption of the synthesized monoliths decreases with respect to their ACF and ACNF precursors (due to lower porosities); however, in volumetric terms H_2 adsorption increases significantly, due to its dependence on both, porosity and material density and thanks to the higher densities reached by the monoliths. Here, the results for the original ACFs can be significantly increased by monolith synthesis, reaching up to 5.5 g l^{-1} and total storage capacities of more than 16.1 g l^{-1}.

References

[1] A. Samanta, A. Zhao, G.K.H. Shimizu, P. Sarkar, R. Gupta, Post-Combustion CO_2 Capture Using Solid Sorbents: A Review, Ind. Eng. Chem. Res. 51 (2012) 1438-1463.

[2] D.M. D'Alessandro, B. Smit, J.R. Long, Carbon dioxide capture: prospects for new materials, Angew. Chem. Int. Ed. 49 (2010) 6058-6082.

[3] N.P. Wickramaratne, M. Jaroniec, Importance of small micropores in CO_2 capture by phenolic resin-based activated carbon spheres, J. Mater. Chem. A 1 (2013) 112-116.

[4] J.P. Marco-Lozar, M. Kunowsky, F. Suárez-García, J.D. Carruthers, A. Linares-Solano, Activated carbon monoliths for gas storage at room temperature, Energy Environ. Sci. 5 (2012) 9833-9842.

[5] J.P. Marco-Lozar, M. Kunowsky, F. Suárez-García, A. Linares-Solano, Sorbent design for CO_2 capture under different flue gas conditions, Carbon 72 (2014) 125-134.

[6] J.P. Marco-Lozar, M. Kunowsky, J.D. Carruthers, A. Linares-Solano, Gas storage scale-up at room temperature on high density carbon materials, Carbon (2014), DOI:10.1016/j.carbon.2014.04.058.

[7] J. Zumerchik, Macmillan Encyclopedia of Energy, Macmillan Reference USA, New York, 2001.

[8] P. Patnaik, Handbook of Inorganic Chemicals, The McGraw-Hill Companies, Inc., New York, 2002.

[9] L. Schlapbach, A. Züttel, Hydrogen-storage materials for mobile applications, Nature 414 (2001) 353-358.

[10] M. Kunowsky, J.P. Marco-Lozar, A. Linares-Solano, Material Demands for Storage Technologies in a Hydrogen Economy, J. Renewable Energy, Article ID 878329 (2013) 1-16.

[11] G.D. Berry, S.M. Aceves, Onboard storage alternatives for hydrogen vehicles, Energy & Fuels 12 (1998) 49-55.

[12] M. Rzepka, P. Lamp, M.A. De La Casa-Lillo, Physisorption of hydrogen on microporous carbon and carbon nanotubes, J. Phys. Chem. B 102 (1998), 10894-10898.

[13] A.M. Seayad, D.M. Antonell, Recent Advances in Hydrogen Storage in Metal-Containing Inorganic Nanostructures and Related Materials, Adv. Mater. 16 (2004) 765-777.

[14] K.L. Lim, H. Kazemian, Z. Yaakob, W.R.W. Daud, Solid-state materials and methods for hydrogen storage: A critical review, Chem. Eng. Technol. 33 (2010) 213-226.

[15] M. Jordá-Beneyto, M. Kunowsky, D. Lozano-Castelló, F. Suárez-García, D. Cazorla-Amorós, A. Linares-Solano, Hydrogen Storage in Carbon Materials, in: A.P. Terzyk, P.A. Gauden, P. Kowalczyk (Eds.), Carbon Materials – Theory and Practice, Research Signpost, Kerala, 2008, pp. 245-281.

[16] A. Linares-Solano, D. Lozano-Castelló, M.A. Lillo-Ródenas, D. Cazorla-Amorós, Carbon activation by alkaline hydroxides: preparation and reactions, porosity and performances, in: Chemistry & Physics of Carbon, Volume 30, 2008, pp. 1-62.

[17] F. Suarez-García, M. Jordá, D. Lozano-Castelló, D. Cazorla-Amorós, A. Linares-Solano, Hydrogen adsorption on carbon materials at high pressures and different temperatures, in: Recent Advances in Adsorption Process, Springer, 2008, pp. 165-175.

[18] A. Linares-Solano, D. Cazorla-Amorós, Adsorption on Activated Carbon Fibers, in: Adsorption by Carbons, Elsevier Ltd., 2008, pp. 431-449.

[19] A. Linares-Solano, M.A. Lillo-Ródenas, J.P. Marco-Lozar, M. Kunowsky, A.J. Romero-Anaya, Utility of sodium and potassium hydroxides for preparing superior quality activated carbons, in: Hydroxides: Synthesis, Types and Applications, Nova Science Publishers, 2012, pp. 73-104.

[20] A. Linares-Solano, D. Cazorla-Amorós, J.P. Marco-Lozar, F. Suárez-García, High pressure gas storage on porous solids; a comparative study of MOFs and activated carbons, in: Coordination Polymers & MOFs, Nova Science Publishers, 2012, pp. 197-223.

[21] A. Linares-Solano, D. Cazorla-Amorós, Activated Carbon fibers, in: Handbook of Advanced Ceramics, Academic Press: Elsevier Inc., second ed, 2013, pp. 155-169.

[22] D. Lozano-Castelló, F. Suárez-García, A. Linares-Solano, D. Cazorla-Amorós, Advances in hydrogen storage in carbon materials, in: Renewable Hydrogen Technologies: Production, Purification, Storage, Aplications and Safety, Elsevier, 2013, pp. 269-291.

[23] J. Alcañiz-Monge, D. Lozano-Castelló, D. Cazorla-Amorós, A. Linares-Solano, Gas storage - adsorbed natural gas (ANG) & hydrogen storage, in: Green Carbon Materials: Advances and Applications, Pan Stanford, 2013.

[24] R. Chahine, T.K. Bose, Low-pressure adsorption storage of hydrogen, Int. J. Hydrogen Energy 19 (1994) 161-164.

[25] M. Kunowsky, F. Suárez-García, A. Linares-Solano, Adsorbent density impact on gas storage capacities, Micropor. Mesopor. Mater. 173 (2013) 47-52.

[26] M. Kunowsky, J.P. Marco-Lozar, D. Cazorla-Amorós, A. Linares-Solano, Scale-up activation of carbon fibres for hydrogen storage, Int. J. Hydrogen Energy 35 (2009) 2393-2402.

[27] A. Oya, N. Kasahara, Preparation of thin carbon fibers from phenol-formaldehyde polymer micro-beads dispersed in polyethylene matrix, Carbon 38 (2000), 1141-1144.

[28] D. Hulicova, A. Oya, The polymer blend technique as a method for designing fine carbon materials, Carbon 41 (2003) 1443-1450.

[29] M. Kunowsky, J.P. Marco-Lozar, A. Oya, A. Linares-Solano, Hydrogen storage in CO_2-activated amorphous nanofibers and their monoliths, Carbon 50 (2012) 1407-1416.

[30] D. Lozano-Castelló, D. Cazorla-Amorós, A. Linares-Solano, D.F. Quinn, Activated carbon monoliths for methane storage: influence of binder, Carbon 40 (2002) 2817-2825.